Frontiers in Heat and Mass Transfer

Tech Science Press

DOI: 10.32604/fhmt.2023.046832

ARTICLE

Impact of Crosswind on Steady-State and Dynamic Performance of Natural Draft Dry Cooling Tower Group: A Numerical Analysis

Xuhui Jiang[1], Xi Zhang[1], Song Wang[1], Ruiqiong Wang[1], Peng Zou[1], Jingzhou Lu[2] and Xiaoxiao Li[2,*]

[1]PowerChina Chongqing Engineering Co., Ltd., Chongqing, 400060, China

[2]Key Laboratory of Low-Grade Energy Utilization Technologies and Systems, Ministry of Education, School of Energy and Power Engineering, Chongqing University, Chongqing, 400044, China

*Corresponding Author: Xiaoxiao Li. Email: xiao.l@cqu.edu.cn

Received: 16 October 2023 Accepted: 05 December 2023 Published: 21 March 2024

ABSTRACT

This study investigates the performance of a natural draft dry cooling tower group in crosswind conditions through numerical analysis. A comprehensive three-dimensional model is developed to analyze the steady-state and dynamic behavior of the towers. The impact of wind speed and direction on heat rejection capacity and flow patterns is examined. Results indicate that crosswinds negatively affect the overall heat transfer capacity, with higher crosswind speeds leading to decreased heat transfer. Notably, wind direction plays a significant role, particularly at 0°. Moreover, tower response time increases with higher crosswind speeds due to increased turbulence and the formation of vortices. The response times are generally similar for wind directions of 45° and 90°, but differ when facing 0, where the leeward tower exhibits a shorter response time compared to the windward tower. These findings provide valuable insights into the performance of natural draft dry cooling tower groups under crosswind conditions, which can inform the design and operation of similar systems in practical applications.

KEYWORDS

Natural draft dry cooling tower group; crosswind; dynamic characteristics

Nomenclature

A	Area (m^2)
C	Inertial resistance factor
Cp	Specific heat (J Kg^{-1} K^{-1})
CFL	Courant-Fredrichs-Lewy number
e	Accuracy
L	Minimum scale of meshed cells (m)
m	Mass flow rate (kg s^{-1})
NTU	Number of transfer units
Q	Heat transfer rate (kW)
s	Standard deviation
T	Temperature (°C)

t	Time (s)
ρ	Density, mean density (kg m^{-3})
μ	Viscosity (kg $m^{-1}s^{-1}$)

Greek letters

α	Permeability
δ	Convergence
ε	Efficiency
ρ	Density, mean density (kg m^{-3})
μ	Viscosity (kg $m^{-1}s^{-1}$)

Vectors

$\vec{v}$	Velocity
$\hat{i}, \hat{j}, \hat{k}$	Unit vectors of x-, y-, z-direction in Cartesian coordinate system

Subscripts

a, w	Air side, water side
bl	Bottom layer
cw	Crosswind
in	Inside or inlet
out	outside or outlet
max	Maximum value
min	Minimum value
r	Ratio
ref	Reference value
tot	total
wi	water inlet
z	Local value
0	Initial value

1 Introduction

Due to its numerous advantages, such as water conservation, high reliability, and low environmental pollution, the natural draft dry cooling tower (NDDCT) has gained widespread usage in various thermal power stations located in water-scarce regions [1]. This includes coal-fired power stations, solar thermal power stations, geothermal power stations, and distributed energy systems. However, the cooling performance of the dry cooling tower is significantly affected by environmental factors like crosswind, ambient temperature, humidity, and other related conditions. This is because NDDCT utilizes the natural convection of air density difference between the inside and outside of the tower as the driving force to dissipate heat [2,3].

Crosswind is a significant challenge to the performance of NDDCT, and extensive research has been conducted on the operational characteristics of this type of cooling tower under crosswind conditions [4–6]. Wei et al. [7] leveraged wind tunnel tests with a hot water recirculation system and finned tube heat sink to model the performance of a dry cooling tower. Their findings indicated that the negative pressure distribution at the tower inlet impacts the air flow, thermal plume near the tower outlet, and boundary layer separation near the tower outlet. Sun et al. [8] employed numerical

simulations of a NDDCT under crosswind conditions to evaluate flow and heat transfer features inside and outside the dry cooling tower, which were then compared to experimentally acquired data. Ma et al. [9] applied CFD numerical modeling and analysis to explore the heat transfer performance of a cooling tower under various wind and temperature conditions. Their results suggested that the water temperature at the heat exchanger's outlet is linearly related to ambient temperature but not to crosswind speed. Hooman et al. [10] investigated the impact of crosswinds on the effectiveness of NDDCT through numerical modeling and experimental validation. It was found that the maximum relative error between the two methods was 15%. Goodarzi et al. [11] demonstrated that a new geometry for the dry cooling tower improved its thermal performance under windy conditions, regardless of wind direction. Ahmadikia et al. [12] suggested that installing a water spray system at the heat exchanger inlet can optimize the cooling performance of the dry cooling tower, with higher water spray rates resulting in better cooling. Liu et al. [13] utilized numerical simulations to investigate heat transfer performance enhancement resulting from crosswind effects at the top of a 20 m tall small NDDCT. Their study showed the existence of a high-pressure zone on the top side of the tower, which is the principal factor for the formation of low-pressure zones and vortexes at the bottom of the tower. Additionally, the heat transfer effect of the dry cooling tower could be improved by installing air-conducting equipment at the bottom of the tower [14,15].

The studies mentioned above primarily examine the performance of single cooling towers. However, as thermal power stations become larger in scale, the demand for the cooling capacity of dry cooling towers increases, and as a result, dual-tower dry cooling systems are becoming more common [16–18]. In these systems, the relative positioning of towers means that the crosswind in the air flow field inside and outside of the system differs from that of a single tower. Therefore, it becomes increasingly meaningful to study the characteristics of twin towers. Yang et al. [19] investigated two different arrangements of heat exchangers in an NDDCT and found that the crosswind affects the thermal performance differently in each arrangement. Liao et al. [20] focused on a group of twin towers with varying spacing and found that the heat transfer performance was optimized when the towers were arranged in series. Gu et al. [21] explored the effect of different wind protection structures on the heat transfer performance of a double indirect dry cooling tower and concluded that a wind protection wall was the most effective structure, followed by louvers. Khamooshi et al. [22] studied the performance of three in-line dry cooling towers under different tower spacing and wind speed conditions. They found that the interaction between the towers occurred primarily at the top and bottom, and larger cooling towers provided better protection to windward towers. Jahangiri et al. [23] investigated methods to improve the thermal performance of three aligned dry cooling towers and found that installing a windproof wall and injecting flue gas could enhance heat transfer performance under crosswind conditions.

Understanding the effects of disturbances on the cooling system is essential for maintaining optimal operation and efficiency of the power plant. Therefore, it is crucial to conduct dynamic response analysis to understand the disturbances caused by the crosswind. Li [24] conducted dynamic simulations using the inlet water temperature as a disturbance in a dry cooling tower. The simulation results showed that the outlet water temperature of the cooling tower increases with the rise in inlet water temperature, with a certain level of lag. Dong et al. [25,26] developed a 3D model of a NDDCT and used transient CFD simulations to study the response time during the startup process. Factors such as tower height, base diameter, and ambient temperature were analyzed to determine their effects on the NDDCT startup process. Wu et al. [27] focused on a 660 MW thermal power plant that utilized an indirect dry cooling system and established a transient mathematical model of the cooling system. The study investigated the transient characteristics under changing environmental

temperatures, crosswinds, and power load variations. Zhang et al. [28] used a three-dimensional transient CFD model to analyze the transient flow and heat transfer characteristics of a NDDCT under crosswind generation and disappearance conditions. Their findings indicated that the response time differed depending on the change in crosswind speed.

The above review indicates that the majority of studies on NDDCT under crosswind conditions have focused on single towers. Furthermore, the existing research on dry cooling towers mostly centers around steady-state analysis, with limited attention given to dynamic response analysis. To address these concerns, this study focuses on a group of NDDCTs consisting of twin towers. This allows for an investigation of the interaction between the two towers and provides a more comprehensive understanding of the performance of the cooling system as a whole. A CFD numerical model is developed to analyze the variations in the airflow distribution, temperature distribution, and pressure distribution both inside and outside the towers. The analysis is conducted under different wind speeds and directions, including scenarios with and without crosswinds. By examining the dynamic response of the NDDCT group under crosswind conditions, this study offers valuable insights into the system's behavior under various operating scenarios and disturbances.

2 Numerical Method

In this study, numerical analysis methods are employed to develop a three-dimensional CFD numerical model of a NDDCT group. A high-performance server is used to perform the analyses. The CFD solver package ANSYS Fluent is utilized to obtain the airflow and heat transfer characteristics of the tower under crosswind conditions.

2.1 Geometric Modeling and Meshing

The numerical model is created by building the NDDCTs at the center of a cylindrical fluid computational domain with a diameter of 200 meters and a height of 160 meters. The spacing between the twin towers is set to 1.5 times the diameter at the bottom of a single tower. The height of the computational domain is 8 times the height of the tower, and the diameter is 16 times the diameter of the inlet at the bottom of a single tower (which is more than 6 times the equivalent diameter of the twin towers). This ensures that backflow does not occur at the external boundary [2]. The geometric modeling of the numerical model is illustrated in Fig. 1. The detailed parameters of the cooling tower is shown in Table 1.

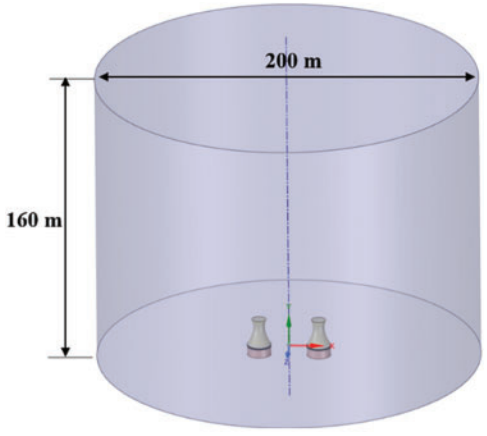

Figure 1: Computation domain of the NDDCTs

Table 1: The parameters of the cooling tower

Parameter configuration	
Environmental design temperature	293.15 K
Tower bottom diameter	12.52 m
Tower height	20 m
Tower top diameter	7.4 m
Number of radiators	18
Total water mass flow rate in each radiator	0.8611 kg/s
Water inlet temperature	352.15 K

In this paper, a multi-region meshing approach is utilized, and a hexahedral structured mesh is employed. As shown in Fig. 2, the minimum edge size is set to 0.3 m and the average mesh size of the cooling tower is set to 0.5 m. To optimize computational resources without compromising the accuracy of calculations, a size gradient meshing method is applied for the external fluid domain. The mesh size near the cooling tower is set to 0.5 m, while the mesh size near the boundary is set to 5 m. This method ensures that the mesh density gradually decreases according to the principle of NDDCT. After conducting grid-independence verification, the final number of grids used in the simulation is approximately 4 million.

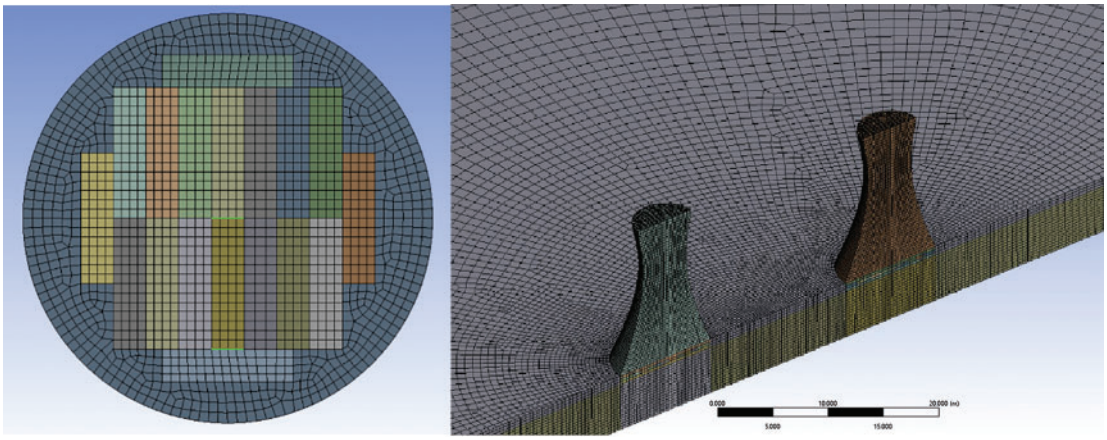

Figure 2: Mesh characteristics

2.2 Turbulence Equations and Boundary Conditions

The fluid in this paper is incompressible, and the equations governing the flow process consist of continuity equations, momentum and energy equations, and turbulence equations as shown in Eq. (1) and Table 2.

$$\frac{\partial \rho \Phi}{\partial t} + \nabla \left(\rho \vec{v} \Phi \right) = \nabla \left(\Gamma_{\Phi} \nabla \Phi \right) + S_{\Phi} \tag{1}$$

Table 2: Summary of governing equations

Equation	Φ	Γ_Φ	S_Φ
Mass conservation	1	0	0
Conservation of momentum in the x-direction	U	μ_e	$-\frac{\partial p}{\partial x}+\nabla\left(\mu_e\frac{\partial}{\partial x}\cdot\vec{v}\right)+F_x$
Conservation of momentum in the y-direction	V	μ_e	$-\frac{\partial p}{\partial y}+\nabla\left(\mu_e\frac{\partial}{\partial y}\cdot\vec{v}\right)+F_y$
Conservation of momentum in the z-direction	W	μ_e	$-\frac{\partial p}{\partial z}+\nabla\left(\mu_e\frac{\partial}{\partial z}\cdot\vec{v}\right)+F_z$
Energy Conservation	T	$\frac{K_e}{C_p}$	$\frac{1}{C_p}\left(\frac{qA_c}{V_C}\right)$
Turbulent kinetic energy k	k	$\mu+\frac{\mu_t}{\sigma_k}$	$G_K+G_b-\rho\varepsilon$
Dissipation rate ε**	ε	$\mu+\frac{\mu_t}{\sigma_\varepsilon}$	$\rho C_1 S\varepsilon+\rho C_2\frac{\varepsilon^2}{k+\sqrt{v\varepsilon}}+C_{1\varepsilon}C_{3\varepsilon}G_b\frac{\varepsilon}{k}$

In the equation, for the Realizable k $-$ ε turbulence model, there are:

$$\mu_e=\mu+\mu_t,\mu_t=\rho C_\mu\frac{k^2}{\varepsilon},K_e=K+K_t,K_t=\frac{C_p\mu_t}{\mathrm{Pr}_t};$$

$$G_k=\mu_t S^2,G_b=\rho g\frac{\mu_t}{\mathrm{Pr}_t}\frac{\partial T}{\partial y},\beta=\left.\frac{1}{T_0}\right|_{P_0};C_1=\max\left[0.43,\frac{\eta}{\eta+5}\right],\eta=S\frac{k}{\varepsilon},S=\sqrt{2S_{ij}S_{ij}};$$

$$C_{1\varepsilon}=1.44,C_2=1.9,\sigma_k=1.0,\sigma_\varepsilon=1.2,C_{3\varepsilon}=\tanh\left(\frac{V}{U}\right);$$

$$\mathrm{Pr}=0.74,\mathrm{Pr}_t=0.85,T_0=293.15.$$

In this paper, the Realizable k$-\varepsilon$ equation and the Standard wall function are used to describe the turbulent flow process of air in the NDDCT. Compared with the traditional Standard k$-\varepsilon$ equation, it can more accurately predict the flow conditions including rotation, reflux, and boundary layer under a large pressure gradient. This has been demonstrated to be suitable for simulating the air flow in the NDDCT [2,25,26,29,30].

The boundary conditions of the numerical model are set as shown in Fig. 1. Under windy conditions, the windward side of the computational domain is set as the velocity inlet boundary condition, the leeward side is set as the pressure outlet boundary condition, and the top surface is set as the symmetry surface. The two sides of the calculated area were set as the pressure inlet boundary conditions and the upper surface as the pressure outlet boundary conditions in the no-wind condition. The bottom ground in both cases is set as the adiabatic wall boundary, and the cooling tower shell and the supporting frame of the internal heat exchanger are set as the no-slip adiabatic wall boundary conditions, using the standard wall function.

The turbulent dissipation rate at the velocity inlet boundary is defined as:

$$\varepsilon=\rho c_\mu\frac{k^2}{\mu}\left(\frac{\mu_t}{\mu}\right)^{-1} \tag{2}$$

where, c_μ is an empirical constant, which usually takes the value of 0.09 at the inlet boundary, and $\frac{\mu_t}{\mu}$ is the turbulent viscosity ratio, which is usually set to a smaller value in external free flows with low turbulence levels, and takes the value of 1.1 in this paper.

The turbulent kinetic energy k at the velocity inlet boundary is defined as follows:

$$k = 1.5\left(u_{\text{avg}} I\right)^2 \tag{3}$$

where, u_{avg} is the mean velocity and I is the turbulence intensity, which is taken as 10% in this paper.

In steady-state calculations, the inlet wind speed is a time-independent function and follows a power-exponential distribution.

$$v_z = v_{ref}\left(\frac{Z}{Z_{ref}}\right)^{0.2} \tag{4}$$

where v_{ref} is the reference wind speed at the standard wind speed observation height Z_{ref}, the exponential power is taken as 0.2, and the crosswind speeds in other directions are all zero, $v_x = v_y = 0$ m/s.

In the transient calculation, the expression of the wind speed function of the velocity inlet boundary needs to introduce the relevant time term. For ease of calculation, the process of lateral wind change is regarded as a linear increase [28]. Assuming that the wind speed increases linearly to a certain value within 10s after the crosswind appears and then remains constant, the time-dependent inlet velocity profile on the velocity inlet boundary can be expressed as follows:

Velocity entry profile during crosswind generation:

$$V(t) = \begin{cases} \frac{v_z}{10}(t) & 0 \le t \le 10 \\ v_z & t > 10 \end{cases} \tag{5}$$

2.3 Solution Algorithm

In this paper, the ambient air is assumed to be an incompressible ideal gas. The buoyancy-driven flow with natural convection is modeled using the Boussinesq assumption. The heat exchanger is simplified to a rectangular structure for modeling purposes. To account for the temperature stratification phenomenon of the water in the heat exchanger during the flow process, the Macro Heat Exchanger (MHE) model is used for the finned tube bundle of the heat exchanger. Furthermore, the exothermic process of the circulating water in the heat exchanger is not completely uniform and is taken into consideration in the MHE model. This model allows for a more accurate prediction of the heat transfer performance of the heat exchanger under such conditions.

In the MHE model, the heat transfer performance of a single cell is calculated by:

$$Q_{cell} = \varepsilon\left(mc_p\right)_a\left(T_{\text{in,auxiliary}} - T_{a1,\text{cell}}\right) \tag{6}$$

where ε is the heat exchanger effectiveness and can be expressed as

$$\varepsilon = 1 - \exp\left\{-\frac{1}{C_r} NTU^{0.22}\left[1 - \exp\left(-C_r NTU^{0.78}\right)\right]\right\} \tag{7}$$

where C_r is the ratio of the heat capacity rate of air to that of water, NTU is the number of transfer units.

$$NTU = \frac{KA}{m_a c_{pa}} \tag{8}$$

where K and A are the heat transfer coefficient and areas of the air-cooled heat exchangers, these value of the two is correlated based on the experimental data of the heat exchanger.

The heat rejection rate from a macro is derived by adding the heat transfer rates of all the cells inside the macro, as illustrated in:

$$Q_{\text{macro}} = \sum Q_{\text{cell}} \tag{9}$$

In transient calculations, the time step is an important parameter that has a large impact on the simulation results. It is defined as:

$$\Delta t = CFL\frac{L}{V} \tag{10}$$

where L is the minimum size of the grid cell, V is the characteristic velocity, and CFL is the number of judgments of the convergence condition. As for the selection of the time step, this paper determines it to be 0.1 s after referring to the previous research.

For the discretization format, second-order windward discretization is employed. This discretization scheme provides better accuracy and stability compared to lower-order schemes. In transient calculations, the PISO (Pressure-Implicit with Splitting of Operators) algorithm is utilized as the pressure-velocity coupling algorithm. The PISO algorithm is particularly suitable for unsteady flow simulations and offers improved stability and faster convergence. By utilizing these algorithms and discretization methods, the paper aims to obtain reliable and efficient solutions for the flow calculations, both in steady-state and transient scenarios.

2.4 Model Validation

2.4.1 Grid and Time Steps Independence Verification

In this paper, mesh independence analysis was performed to ensure that the numerical results are not affected by the sparsity of the mesh used for simulations. To this end, six different models were created with varying numbers of grid points, and steady-state calculations were performed under two wind speed conditions for each model. The stabilized heat transfer data were then obtained for all models. Fig. 3 in the paper shows the results of this analysis, which indicates that when the number of grids exceeds 4.0 million, the change in the number of grids has a negligible impact on the calculation results. Based on these findings, a model with 4.0 million grid points was selected for subsequent calculations to strike a balance between computational efficiency and accuracy.

The heat transfer rates of the cooling tower at different time steps were compared to assess the independence of time steps in our simulation. We conducted a comprehensive analysis and provided a detailed comparison of the heat transfer rates at various time steps, ranging from 0.1 to 0.5 s. The findings are presented in Fig. 4. As can be seen in the figure, the heat transfer rate remains consistent when the time step is smaller than 0.2 s. This consistency implies that our simulation is indeed independent of the time step size.

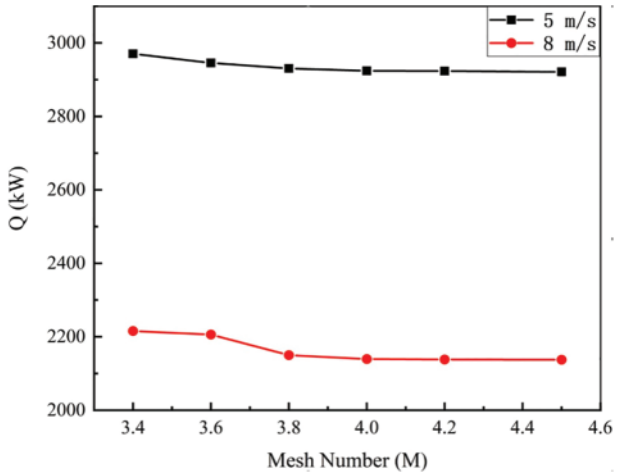

Figure 3: Mesh independence verification

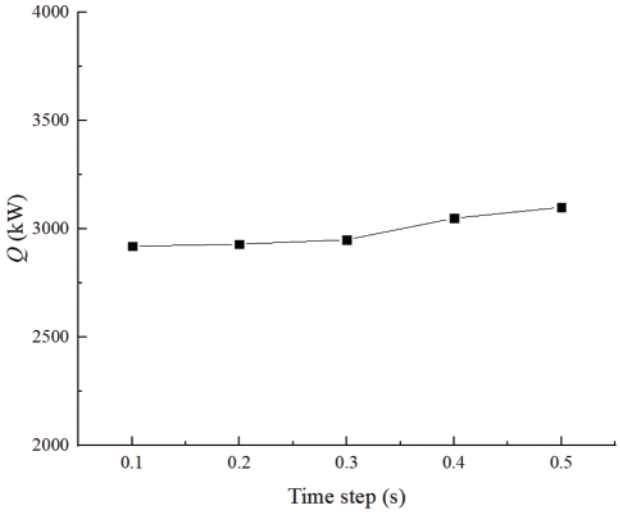

Figure 4: Time step independence verification

2.4.2 Model Validation

Experimental verification is an important step in validating the accuracy of numerical simulations. However, in the case of transient heat transfer characteristics in cooling towers, there is currently limited experimental research information available. Therefore, in this paper, the steady-state calculation results are verified with experimental data obtained from a small NDDCT built by a previous researcher. The experimental cooling tower has a height of 20 meters. The steady-state performance, including ambient temperature, cooling tower inlet temperature, and cooling tower outlet temperature, is tested under different crosswind speeds of 2.23, 5.56, and 8.34 m/s, respectively. Table 3 presents the details of the experimental verification. The table shows the difference between the simulated steady-state results and the experimental data, with the maximum error controlled within 5%. This indicates that the simulation results are in good agreement with the experimental findings and within an acceptable range of error.

Table 3: Comparison of steady-state data and experimental data

Case	Crosswind speed (m/s)	Ambient temperature (K)	Water inlet temperature (K)	Water outlet temperature (K) (Test|Model)	Error
1	2.23	296.82	353.13	317.62|316.65	2.17%
2	5.56	293.39	336.17	312.69|313.08	3.5%
3	8.34	289.74	325.77	305.58|307.05	4.5%

3 Results and Discussion

3.1 Steady-State Characterization of Natural Draft Dry Cooling Tower Groups under Crosswind Conditions

In this paper, the steady-state characteristics of the NDDCT group are investigated in the presence of crosswind. The paper analyzes the changes in the distribution of the airflow field, pressure field, and temperature field inside and outside the tower group under different wind speeds (0, 3, 5, 8, and 10 m/s) and wind directions (0°, 45°, and 90°). By doing so, the coupling mechanism is examined, and the steady-state flow and heat transfer characteristics of the tower group are summarized. Fig. 5 presents a schematic diagram of the wind angle, which is used to describe the orientation of the crosswind relative to the tower group.

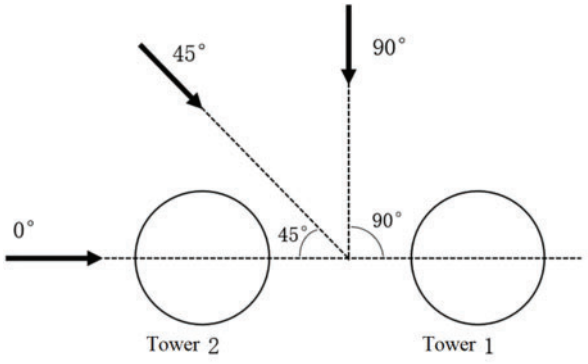

Figure 5: The outline of the wind direction angle

3.1.1 Influence of Crosswind Velocity on the Steady-State Characteristics of Dry Cooling Tower Groups

Table 4 presents the steady-state data of the NDDCT group under different wind speeds and directions. The table shows that the total heat transfer of the NDDCT group exhibits a decreasing trend with an increase in crosswind speed due to the negative influence of crosswind disturbance on the dry cooling tower in all three wind directions. The data also indicates that when the wind speed is less than 3 m/s, the total heat transfer of the NDDCT group changes slowly with the wind speed. However, in the wind speed interval of 3 to 8 m/s, the heat transfer rate experiences a faster change in response to the wind speed. Finally, when the wind speed exceeds 8 m/s, the change in wind speed has a very small impact on the heat exchanger of the dry cooling tower.

Table 4: The influence of wind speed on the total heat transfer rate (kW) of NDDCTs

Wind speeds		0 m/s	3 m/s	5 m/s	8 m/s	10 m/s
Wind directions						
90°	Tower 1	1900.7	1836.6	1464.3	1074.8	1062.4
	Tower 2	1900.8	1834.1	1465.3	1081.1	1068.2
	Total	3801.5	3670.7	2929.5	2155.9	2130.6
45°	Tower 1	1901.6	1842.1	1526.1	1167.2	1150.5
	Tower 2	1901.7	1853.7	1567.8	1214.2	1177.5
	Total	3803.3	3695.8	3093.9	2381.4	2328.0
0°	Tower 1	1900.0	1826.0	1639.3	1415.8	1359.0
	Tower 2	1900.2	1860.8	1537.0	1116.0	1059.5
	Total	3800.2	3686.8	3176.3	2531.7	2418.5

Fig. 6 depicts the air flow details of the dry cooling tower group at different wind speeds (0, 3, 5, 8 m/s) when the wind direction is 90°. When there is no crosswind, natural convection occurs as the air at the bottom of the tower is driven by the density difference formed by heat dissipation of the heat exchanger. This air flows into the tower through the heat exchanger and exits vertically upwards. However, the introduction of crosswinds changes the airflow inside the dry cooling tower group. As the crosswind speed increases, the airflow undergoes a series of changes. When the wind speed reaches 8 m/s, a vortex appears on the windward side of the tower, causing hot air to be trapped inside the tower rather than being discharged out of the tower through the heat exchanger. This reduces the temperature difference between the air and the surface of the heat exchanger, impeding the heat transfer between the heat exchanger circulating water and the cold air.

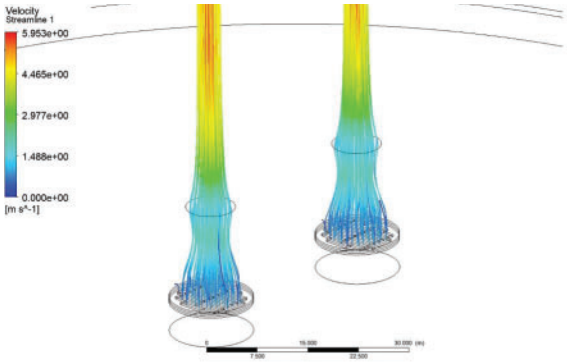

(a) 0 m/s

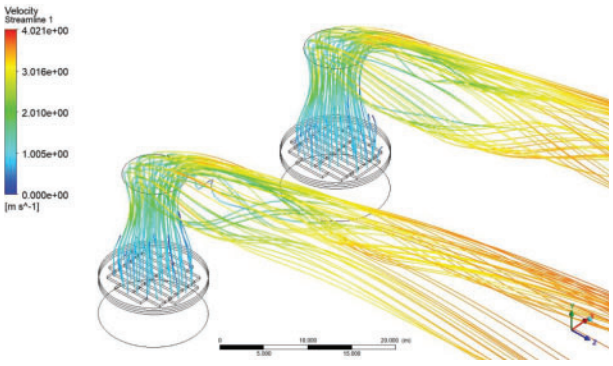

(b) 3 m/s

Figure 6: (Continued)

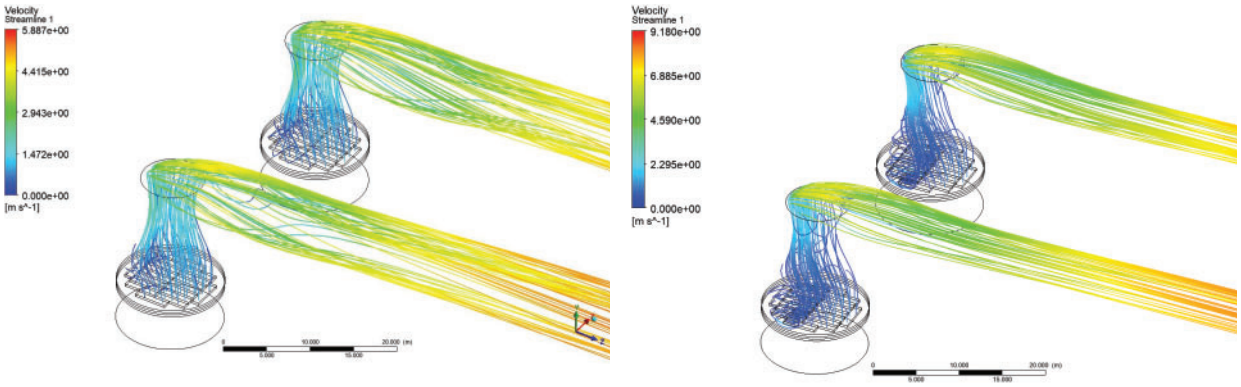

(c) 5 m/s (d) 8 m/s

Figure 6: Streamlines of NDDCTs under different crosswind wind speeds

3.1.2 Influence of Crosswind Direction on the Steady-State Characteristics

Unlike a single NDDCT simulation, in the study of a group of towers, the wind direction of the ambient crosswind has an important influence on the flow heat transfer characteristics of the group due to the relative position of the dry cooling towers. This subsection will focus on the effect of wind direction on the steady-state characteristics of the tower group from the perspective of the interaction between the two dry cooling towers.

According to the data presented in Table 4, under the 90° wind direction, the heat rejection rate of both dry cooling towers remains consistent across all wind speeds. When considering the 45° wind direction, the heat transfer performance between the two towers is similar at low wind speeds. However, at higher wind speeds (5, 8, and 10 m/s), Tower 2 exhibits a higher heat transfer compared to Tower 1, with differences of 2.7%, 4.0%, and 2.3%, respectively. In the case of the 0° wind direction, upon analyzing different wind speeds (3, 5, 8, 10 m/s), it was observed that the leeward tower (Tower 1) exhibited a higher heat transfer rate compared to the windward tower (Tower 2) by −1.9%, 6.7%, 26.9%, and 28.3%, respectively.

Based on Fig. 7, which displays the pressure and flow field distribution at the bottom of the NDDCT group under three crosswind wind directions at a wind speed of 5 m/s, it can be observed that the interaction between the flow fields inside and outside the two NDDCTs is minimal in the cases of 90° and 45° wind directions. The air flow and heat transfer characteristics inside and outside each NDDCT resemble those of a single tower, as shown in Figs. 7a and 7b. Fig. 7c reveals that the presence of the two adjacent dry cooling towers has an impact on the flow field of the windward tower (Tower 2) but does not significantly affect the flow field under other wind directions. On the other hand, the flow field of the leeward tower (Tower 1) is influenced by the windward tower's flow field. The wind blowing across the leeward tower is blocked by the windward tower, resulting in reduced airflow velocity near the windward side of the heat exchanger bottom of Tower 1, as indicated in Fig. 7a. Due to this blocking effect, the negative pressure zone of Tower 1 is diminished compared to that of the windward tower. Consequently, the airflow rate into Tower 1 through the heat exchanger increases, enhancing the cooling capacity of Tower 1. Furthermore, as depicted in Fig. 8, the tail flow generated by the plume at the top outlet of the windward tower, redirected by the crosswind, weakens the interference of the strong crosswind on the top outlet of the leeward tower. This results in lower

airflow velocity near the outlet of the leeward tower and reduces the overall impact of the crosswind on Tower 1. As a result, the heat exchange capacity of Tower 1 is improved.

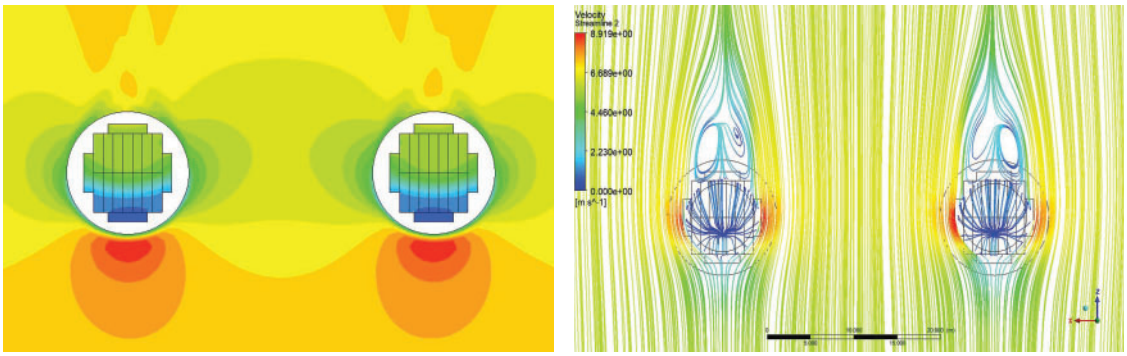

(a) 90°

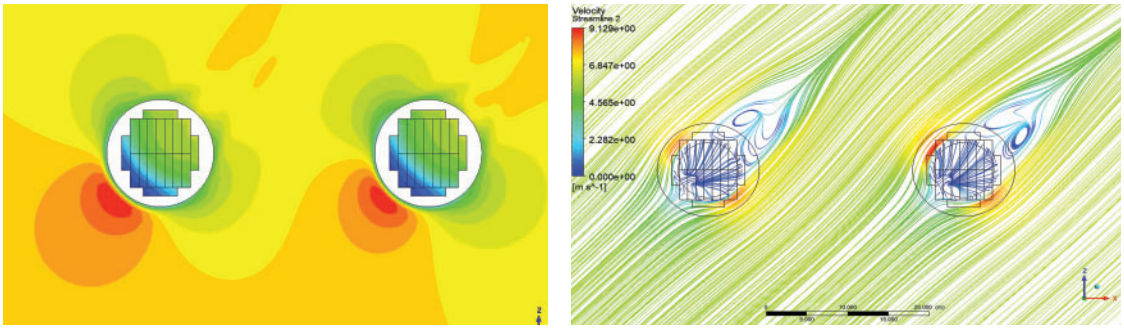

(b) 45°

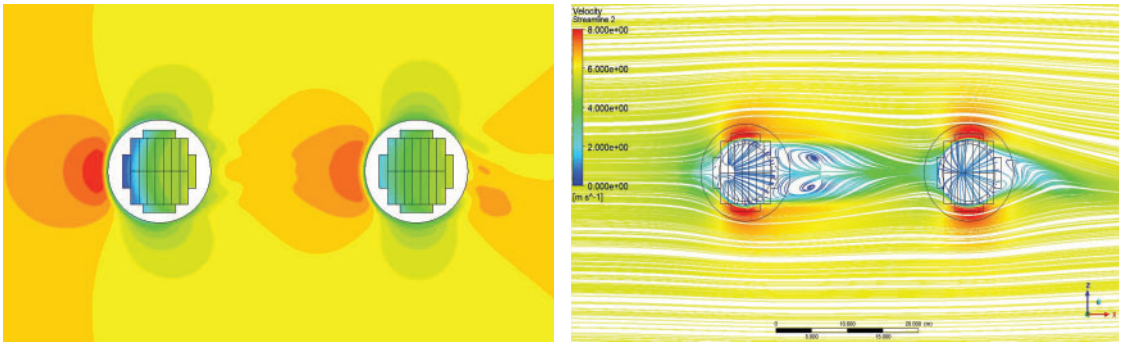

(c) 0°

Figure 7: The flow field of NDDCTs under different crosswind wind direction with the speed of 5 m/s

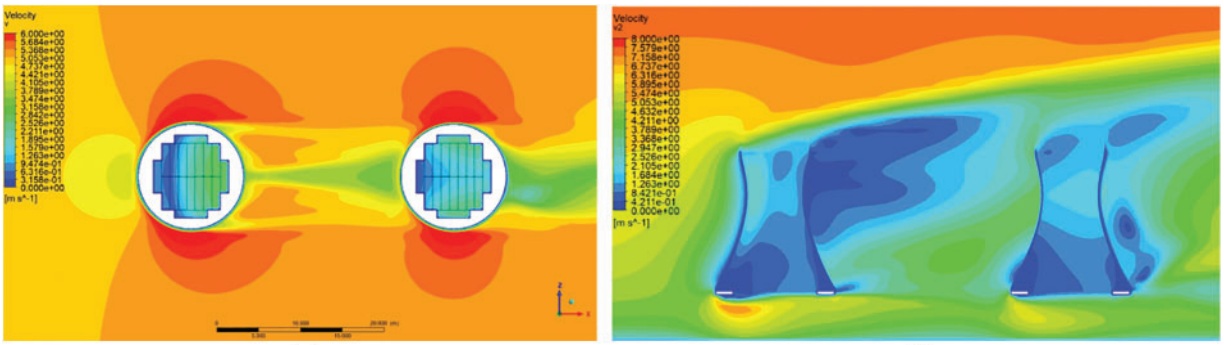

(a) (b)

Figure 8: The air velocity of NDDCTs under the condition of 0° wind direction and 5 m/s wind speed (a) the inlet height of heat exchanger, (b) the middle section of towers

In summary, the influence of wind direction on the dry cooling tower group is most obvious in the 0° wind direction. The obstruction effect of the windward tower on the crosswind makes the wind speed decrease when the crosswind reaches the location of the windward tower, the gradient of air pressure distribution at the bottom of the tower decreases, the pressure difference between the air at the bottom of the tower and the air above the heat exchanger in the tower increases, the air mass flow into the tower increases, and it can be smoothly flowed out from the top outlet of the tower, which reduces the average temperature inside the windward tower, and the heat dissipation capacity of the heat exchanger is enhanced, so the amount of heat exchanged is increased.

3.2 Dynamic Characterization of NDDCT Groups under Crosswind Conditions

In this section, we simulate the dynamic response of the NDDCT group under crosswind conditions. When subjected to the emerge of the crosswind, the heat rejection capacity of the cooling towers is disrupted and undergoes changes until it eventually reaches a new stable state. The time it takes for the system to reach this stability is referred to as the response time. Mathematically, the response time can be defined as follows:

$$\frac{Q(t)-\overline{Q}(t)}{\overline{Q}(t)} \le e \tag{11}$$

That is, when the relative fluctuation between the heat transfer rate as a function of time $Q(t)$ and the stable heat transfer rate $\overline{Q}(t)$ is less than a certain value (10^{-3} in this paper), the NDDCT is considered to have reached a steady state.

Table 5 gives a summary of the dynamic parameters of the dry cooling tower group for different wind speed occurrences in the three wind directions.

Table 5: The dynamic performance of the tower group with crosswind emerged at different speeds

	Wind direction	90°		45°		0°	
	Wind speed	Tower 1	Tower 2	Tower 1	Tower 2	Tower 1	Tower 2
Response period (s)	0–3 m/s	198	201	199	200	190	278
	0–5 m/s	228	224	212	218	220	225
	0–8 m/s	277	276	277	276	275	290
Time-averaged heat transfer rate (kW)	0–3 m/s	1791.4	1788.8	1796.4	1817.5	1818.5	1773.4
	0–5 m/s	1480.0	1446.2	1451.9	1494.3	1619.2	1522.9
	0–8 m/s	1159.3	1124.6	1374.3	1392.4	1377.6	1294.7
Time-averaged temperature (K)	0–3 m/s	319.9	319.8	321.3	321.2	320.4	321.7
	0–5 m/s	320.3	320.3	320.8	320.9	319.5	321.1
	0–8 m/s	318.4	318.4	318.9	318.9	318.1	319.1
Shock amplitude	0–3 m/s	13.6%	14.0%	15.6%	13.5%	14.6%	15.6%
	0–5 m/s	43.5%	42.9%	43.0%	41.1%	39.1%	39.2%
	0–8 m/s	49.9%	49.5%	49.0%	45.3%	49.3%	44.4%

3.2.1 Influence of Crosswind Speed on the Dynamic Characteristics

The above table shows that the dynamic response time of the NDDCT group varies with different wind speeds. The results indicate that as the wind speed increases, the NDDCT group requires more time to reach a new stable operation state than it does when the wind speed is 3 m/s. Specifically, under a wind direction of 90°, the response time of the NDDCT group increases by an average of 13.3% and 38.6% in the presence of wind speeds of 5 and 8 m/s, respectively. Under a wind direction of 45°, the response time of the NDDCT group increases by an average of 7.8% and 38.6% for wind speeds of 5 and 8 m/s, respectively. Similarly, under a wind direction of 0°, the response times for wind speeds of 5 and 8 m/s increase by an average of 4.9% and 20.7%, respectively.

In Fig. 9, the variation curve of the overall heat rejection capacity of the NDDCT group with time is depicted for the 90° wind direction. This curve demonstrates that the behavior of the NDDCT group follows a similar pattern as the steady-state calculation results. As the wind speed increases, the negative impact of the crosswind on the heat dissipation capacity of the NDDCT group becomes more pronounced. Under the 90° wind direction, the steady-state heat transfer capacity decreases by nearly 40% when comparing the variation from 0 to 8 m/s crosswind (2139.0 kW) with the variation from 0 to 3 m/s crosswind (3613.4 kW).

In Fig. 10, the dynamic response of Tower 1's parameters is illustrated for the presence of a 3 m/s crosswind at a wind direction of 90°. After the appearance of the crosswind at $t = 10$ s, the heat rejection capacity and inlet mass flow rate rapidly decrease, reaching their lowest values of 1641.8 kW and 48.4 kg/s, respectively, within approximately 30 s. They then recover quickly to 1824.6 kW and 54.6 kg/s before decreasing again. After several fluctuations, both variables gradually increase and eventually stabilize at values of 1808.2 kW and 56.8 kg/s, respectively. In contrast, the volume-averaged temperature in the dry cooling tower initially experiences a small decrease during the first 10 s after the crosswind appears. It then recovers to the initial temperature level and remains relatively stable for 5 s. At $t = 30$ s, it starts to rapidly increase, reaching a maximum value of 321.2 K. Subsequently, it slowly decreases and eventually stabilizes at 321.1 K.

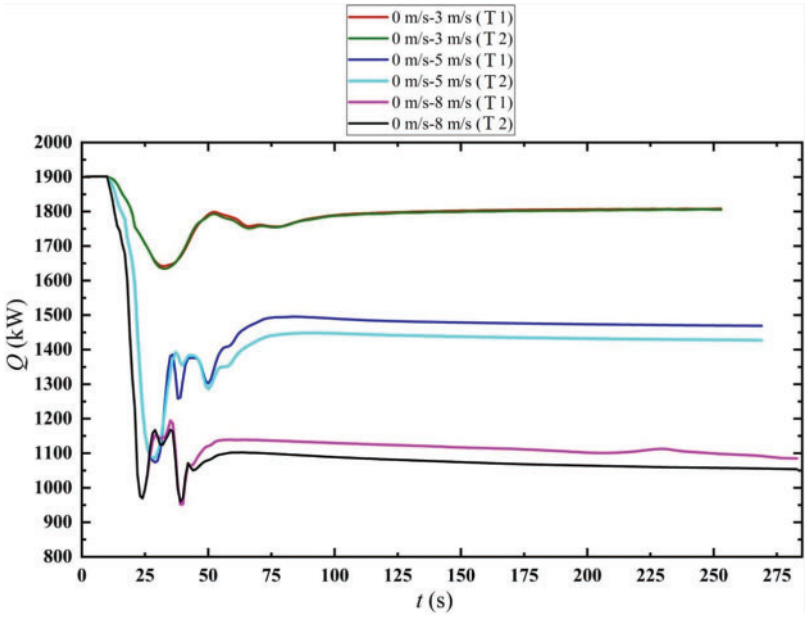

Figure 9: The change of heat transfer rate in the tower under different crosswind conditions

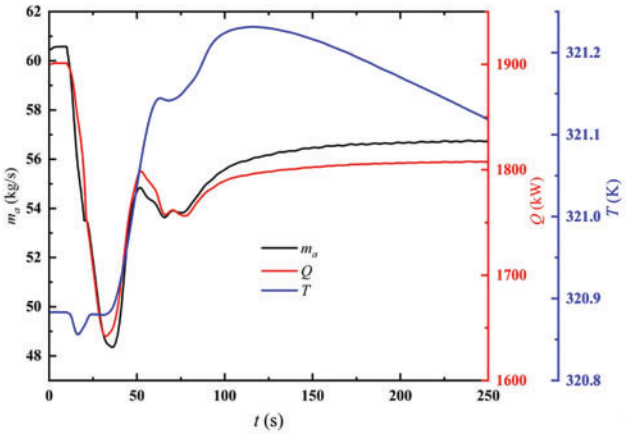

Figure 10: The change of the heat exchanger inlet mass flow rate, heat transfer rate, and the average temperature in the Tower 1 when the crosswind emerged at the speed of 3 m/s

Fig. 11 shows the variation of pressure distribution at the bottom of the dry cooling tower with time. 5 s after the crosswind appears ($t = 10$), the pressure distribution at the bottom of the heat exchanger starts to appear unevenly under the influence of the crosswind, and the negative pressure zone starts to appear at the windward side of the bottom of the dry cooling tower in 21–36 s and gradually expands, and the lowest pressure in the negative pressure zone is −19.3 Pa; the pressure in the negative pressure zone is basically unchanged in 51 s. After 51 s, the pressure in the negative pressure zone remains unchanged. The existence of the negative pressure zone leads to the reduction of the pressure difference between the bottom of the heat exchanger and the inside of the tower, which is why in Fig. 9 the air mass flow into the tower decreases to a minimum of 48.4 kg/s at $t = 36$ s.

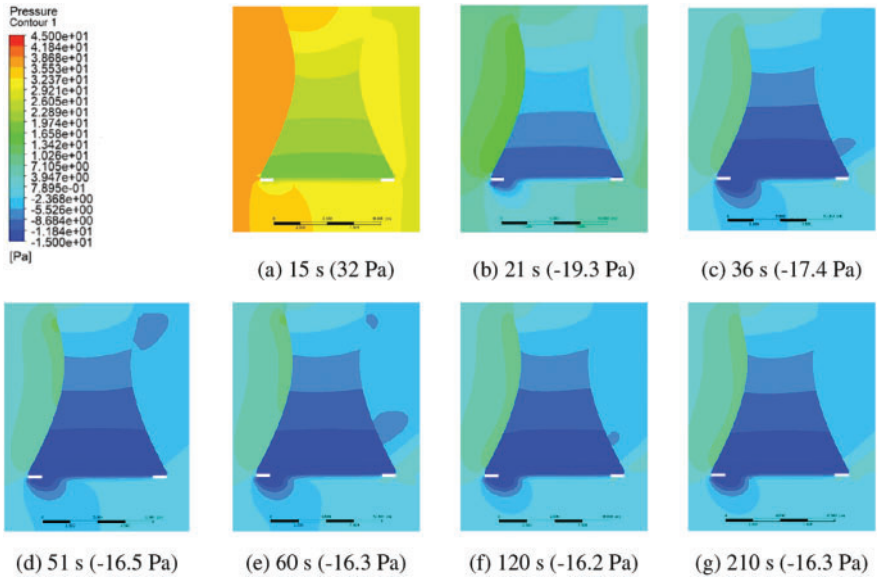

Figure 11: Changes of the pressure contour under different wind speeds

The dynamic responses of the heat transfer capacity, air mass flow rate and volume average temperature in the dry cooling tower at 8 m/s wind speed are analyzed in Fig. 12. Compared to the response observed in Fig. 10 for low wind speeds, the dry cooling tower's response to high wind speeds is more rapid. The heat transfer capacity and heat exchanger inlet mass flow rate drop to extreme values of 969.1 kW and 20.3 kg/s, respectively, within 15 s after the crosswind emerges. From 25 to 60 s, both variables undergo more pronounced oscillations before slowly dropping to a stable value of 1085.3 kW after 60 s. The average temperature in the tower does not change significantly in the first 25 s and then starts to decrease and stabilize at $T = 316$ K after several fluctuations. It is worth mentioning that the response of the dry cooling tower is more drastic in the presence of high wind speeds after the emergence of the crosswind and response time is longer because the later stages of decline and stabilization take longer.

Fig. 13 gives the variation of the flow line diagram of the dry cooling tower group with time, and it can be seen that, unlike the case of the appearance of the low-speed crosswinds, the high-speed crosswind leads to the emergence of vortices on the internal windward side of the tower and at the top outlet successively, and then the vortices in the tower exist all the time, and the vortices at the top outlet have disappeared at 50 s. The vortex at the top causes the air at the top of the tower to pour into the tower, and the cold air causes the local temperature at the top of the tower to drop sharply, but it also hinders the outflow of the hot air inside the tower, and due to the successive dominant roles of the two, the average temperature of the tower fluctuates in the period of time when the crosswind has just appeared. The negative pressure zone on the windward side at the bottom of the tower causes the air inside the tower to flow downward from the heat exchanger, forming a violent vortex, causing the air mass flow rate at the inlet of the heat exchanger to decrease sharply, deteriorating the heat transfer of the heat exchanger, making the heat transfer in the case of a high wind speed occurrence lower than that in the case of a low wind speed occurrence. When the vortex at the top disappears, the air flow at the top outlet of the tower becomes smoother, the heat is discharged from the tower, and the average temperature continues to decrease and eventually stabilizes.

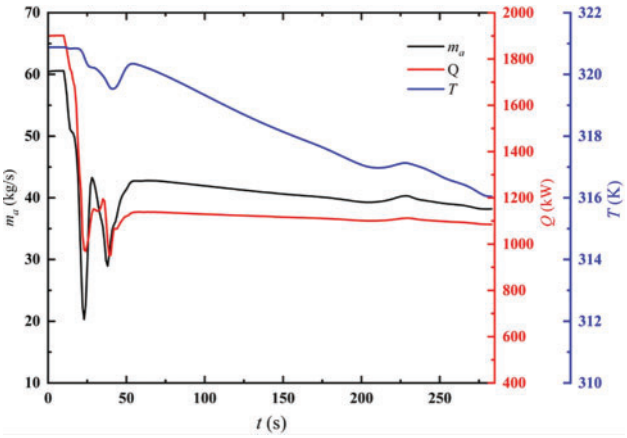

Figure 12: The change of the heat exchanger inlet mass flow rate, heat transfer rate, and the average temperature in Tower 1 when the crosswind emerged at the speed of 8 m/s

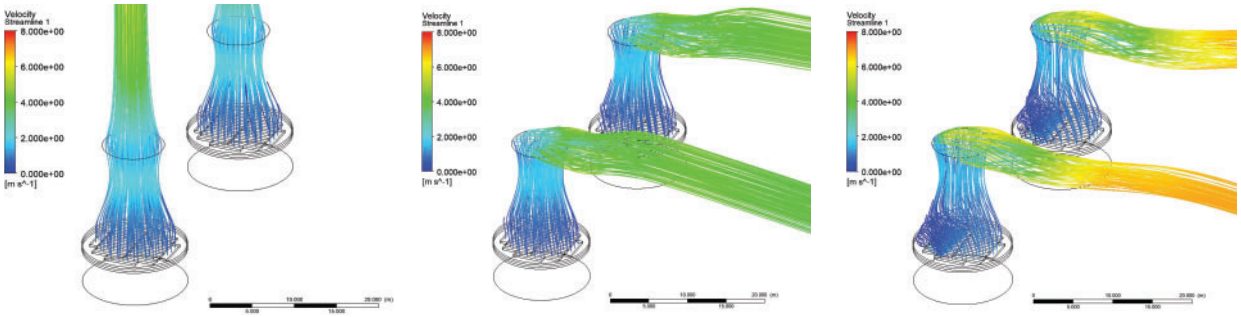

(a) 3 s (b) 15 s (c) 18 s

(d) 3 s (e) 15 s (f) 18 s

Figure 13: Comparison of internal and external airflow patterns in nddcts with crosswind speed of 3 m/s and wind direction of 90°

3.2.2 Influence of Crosswind Direction on the Dynamic Characteristics

From the simulation results presented in Table 5, it can be observed that the response time of both towers to crosswind disturbances is relatively consistent for wind directions of 45° and 90°. This suggests that the interaction between the two dry cooling towers is weak under these wind directions. However, when the wind direction is 0°, there is a noticeable difference in the dynamic response

time between Tower 1 and Tower 2 to the crosswind. This discrepancy becomes more significant at lower wind speeds. For instance, with a 3 m/s wind speed, the leeward tower (i.e., Tower 2) exhibits a shortened response time by approximately 32% compared to the windward tower (i.e., Tower 1). Notably, this difference diminishes to around 5% when higher wind speeds are present (e.g., 8 m/s). The contrasting response times between the windward and leeward towers in the case of a 0° wind direction suggest that the windward tower experiences a delayed response to the crosswind due to the obstructive effects caused by the leeward tower itself. As a result, the leeward tower responds more rapidly to the crosswind disturbance. However, as the wind speed increases, the influence of the leeward tower on the windward tower diminishes, leading to a reduction in the discrepancy in their response times. Since the differences between the twin towers are more obvious at low wind speeds, this section will mainly analyze them from the perspective of the corresponding differences in the dynamic response of the cooling towers when a 3 m/s crosswind occurs in the 0° wind direction.

The results depicted in Fig. 14 illustrate the time-dependent changes in heat transfer capacity, heat exchanger inlet mass flow rate, and average temperature within the two NDDCTs. It is observed that the average temperature trends of the two towers exhibit opposite behaviors after approximately 30 s. Tower 1 demonstrates a gradual decrease in average temperature followed by stabilization, whereas Tower 2 experiences a progressive increase in average temperature before reaching a stable state. Additionally, the variation in mass flow rate at the inlet of the heat exchanger aligns with the trend observed in the heat transfer capacity. This indicates that the changes in heat exchanger inlet mass flow rate correspond to the alterations in heat transfer capacity within the NDDCTs.

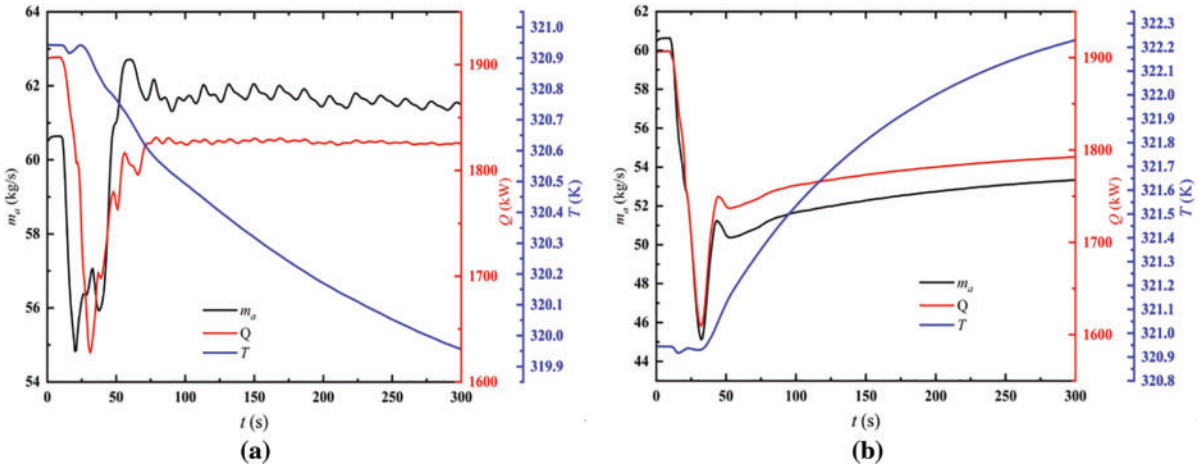

Figure 14: The change of the heat exchanger inlet mass flow rate, heat transfer rate, and the average temperature in (a) Tower 1 (b) Tower 2 when crosswind emerged with the speed of 3 m/s

In Figs. 15 and 16, the pressure distribution and temperature distribution plots of the tower group under a 0° wind direction and 3 m/s wind speed are presented. Within the first 10 s after the crosswind emerges, a negative pressure area forms at the bottom of the tower, leading to a rapid reduction in the airflow entering the tower. From Fig. 15, it can be observed that between 24 and 54 s, the negative pressure area decreases as the crosswind speed stabilizes, increasing the airflow. After this period, the negative pressure area remains relatively constant, and the amount of air entering the tower stabilizes. However, it is worth noting that the flow of air at both the bottom inlet and top outlet of Tower 1 is influenced by the crosswind passing through Tower 2, which is an important factor to consider. Furthermore, Fig. 15 demonstrates that the airflow at both the bottom inlet and top outlet of Tower

1 is affected by the wake flow generated when the crosswind passes through Tower 2. As a result, the airflow exhibits periodic fluctuations in its mass flow rate.

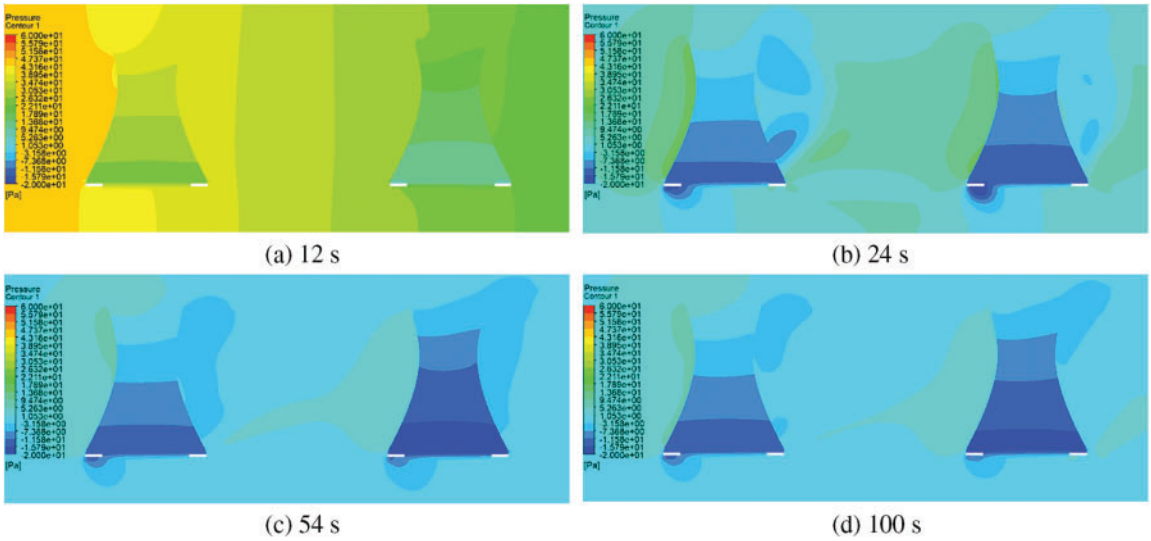

Figure 15: Changes of pressure contour of towers with crosswind speed of 3 m/s and wind direction of 0°

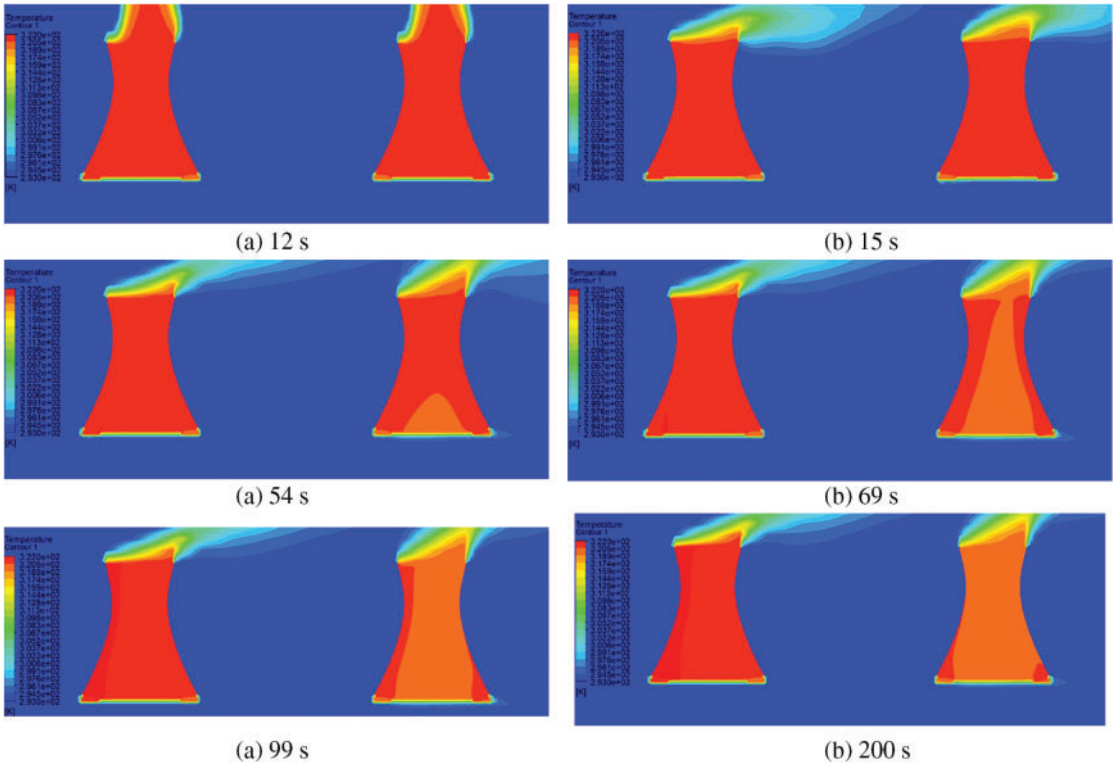

Figure 16: Changes of temperature contour of towers with crosswind speed of 3 m/s and wind direction of 0°

The difference in the variation of the average temperature inside the towers can be attributed to several factors. After 30 s, the airflow into the tower is decreased, which causes a reduction in the heat rejection capability. This situation results in an increasing trend in the temperature within the windward tower, as shown in Fig. 14b. On the other hand, due to the existence of a crosswind pressure gradient within the tower group, Tower 1 is located downstream while Tower 2 is located upstream. As shown in Fig. 17, this leads to a lower pressure inside Tower 1 compared to that inside Tower 2, which, in combination with the blocking effect of the windward tower on the crosswinds, increases the mass flow rate of cold air inhaled into Tower 1. This, in turn, lowers the average temperature inside Tower 1.

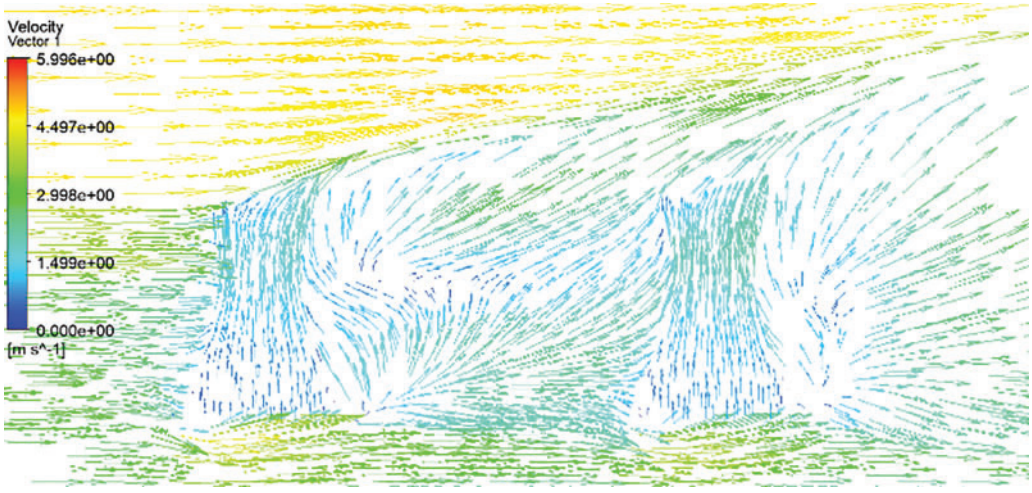

Figure 17: Velocity vectors of the NDDCT group with crosswind speed of 3 m/s and wind direction of 0° ($t = 100$ s)

The results in this section offer valuable insights into the dynamic response of NDDCT groups to varying crosswind conditions, particularly in addressing response time to different wind speeds. The dynamic response of cooling towers can serve as boundary conditions for the control systems of the entire power plant, enabling better monitoring and regulation of the system's operation.

4 Conclusions

In this study, the performance of a natural draft dry cooling tower group under crosswind conditions is investigated by constructing a 3D CFD model. The key findings are as follows:

1. Increasing crosswind speeds negatively impact heat transfer capacity, with the most significant effect observed between 3 to 8 m/s.
2. Heat transfer capacity between twin towers is similar at a wind direction of 90°. However, the obstructive effect of windward towers on crosswinds improved heat transfer performance, resulting in the highest capacity at a wind direction of 0°.
3. Higher crosswind speeds led to longer dynamic response times due to increased turbulence and vortice formation. The response times were generally similar for 45° and 90° wind directions, except at 0° where the leeward tower had a shorter response time than the windward tower.

These findings offer valuable insights into the performance of natural draft dry cooling tower groups under crosswind conditions, facilitating their design and optimization for various applications.

Acknowledgement: The authors would like to express sincere gratitude to the Key Laboratory of Low-grade Energy Utilization Technologies and Systems and Natural Science Foundation of Chongqing for their generous financial support.

Funding Statement: This research received funding from Key Laboratory of Low-Grade Energy Utilization Technologies and Systems (LLEUTS-2023001) and the Natural Science Foundation of Chongqing (CSTB2022NSCQ-MSX1470).

Author Contributions: The authors confirm contribution to the paper as follows: study conception and design: Xuhui Jiang, Ruiqiong Wang; data collection: Peng Zou; analysis and interpretation of results: Jingzhou Lu, Xiaoxiao Li; draft manuscript preparation: Xi Zhang, Song Wang, Xiaoxiao Li. All authors reviewed the results and approved the final version of the manuscript.

Availability of Data and Materials: Data will be made available on request.

Conflicts of Interest: The authors declare that they have no conflicts of interest to report regarding the present study.

References

1. Taimoor, A. A., Saeed, U., Rather, S., Al-Shahrani, S., Bamufleh, H. S. et al. (2022). Economic and technical analysis of a hybrid dry cooling cycle to replace conventional wet cooling towers for high process cooling loads. *Energies, 15,* 7986.
2. Li, X., Gurgenci, H., Guan, Z., Wang, X., Xia, L. (2019). A review of the crosswind effect on the natural draft cooling towers. *Applied Thermal Engineering, 150,* 250–270.
3. Pang, H., Zhao, C., Cheng, S., Wang, M., Gao, Q. et al. (2023). Investigation on feasible zone of nozzle spray for pre-cooling the inlet air of natural draft dry cooling tower. *Thermal Science and Engineering Progress, 38,* 101650.
4. Zhang, X., Sun, F., Chen, X., Deng, W., Chen, K. (2022). Impact mechanism of the chip muffler on the cooling performance of super large-scale natural draft wet cooling tower under crosswind. *Applied Thermal Engineering, 213,* 118753.
5. Chen, K., Sun, F., Zhang, L., Chen, X., Zhang, X. (2022). A sensitivity-coefficients method for predicting thermal performance of natural draft wet cooling towers under crosswinds. *Applied Thermal Engineering, 206,* 118105.
6. Ge, W., Fan, J., Liu, C., Li, W., Chen, G. et al. (2019). Critical impact factors on the cooling performance design of natural draft dry cooling tower and relevant optimization strategies. *Applied Thermal Engineering, 154,* 614–627.
7. Wei, Q., Zhang, B., Liu, K., Du, X., Meng, X. (1995). A study of the unfavorable effects of wind on the cooling efficiency of dry cooling towers. *Journal of Wind Engineering and Industrial Aerodynamics, 54,* 633–643.
8. Sun, T., Gu, Z., Zhou, L., Li, P., Cai, G. (1992). Full-scale measurement and wind-tunnel testing of wind loading on two neighboring cooling towers. *Journal of Wind Engineering and Industrial Aerodynamics, 43,* 2213–2224.
9. Ma, H., Si, F., Li, L., Yan, W., Zhu, K. (2015). Effects of ambient temperature and crosswind on thermo-flow performance of the tower under energy balance of the indirect dry cooling system. *Applied Thermal Engineering, 78,* 90–100.

10. Hooman, K. (2015). Theoretical prediction with numerical and experimental verification to predict cross-wind effects on the performance of cooling towers. *Heat Transfer Engineering, 36,* 480–487.
11. Goodarzi, M., Maryamnegari, S. M. (2018). A new natural draft dry cooling tower with improved thermal performance during windy condition. *Applied Thermal Engineering, 139,* 341–351.
12. Ahmadikia, H., Soleimani, M., Gholami, E. (2013). Simultaneous effects of water spray and crosswind on performance of natural draft dry cooling tower. *Thermal Science, 17,* 443–455.
13. Liu, Q., Xia, L., Hu, M., Li, X., Mi, Z. et al. (2018). Positive impact of a tower inlet cover on natural draft dry cooling towers under crosswind conditions. *Applied Thermal Engineering, 139,* 283–294.
14. Abbasi, M., Alighanbari, F., Sarvestani, A. B., Golneshan, A. A. (2022). The effect of crosswind and installation of wind-break deflector on the performance of natural draft dry cooling tower (NDDCT). *Journal of Wind Engineering and Industrial Aerodynamics, 229,* 105146.
15. He, S., Li, Y., Wang, M., Wang, A., Alkhedhair, A. M. et al. (2022). Investigation on the control mechanism of spray pre-cooling the inlet air of natural draft dry cooling tower. *Applied Thermal Engineering, 217,* 119186.
16. Ma, H., Cai, L., Si, F. (2022). Numerical study on the effects of layout compactness of the annular-aligned moist media on thermo-hydraulic performance of an indirect dry cooling tower. *Applied Thermal Engineering, 213,* 118649.
17. Ma, H., Cai, L., Si, F. (2023). Numerical study identifies the interaction between two adjacent dry cooling towers on fluid flow and heat transfer performances of the radiators at different points of each tower. *International Journal of Thermal Sciences, 191,* 108351.
18. Zhao, Y., Zhao, Q., Li, F., Liang, Q., Li, X. et al. (2023). Effect mechanism of cooling delta aerodynamic field equalizing on the cooling characteristics of dry cooling tower. *International Communications in Heat and Mass Transfer, 148,* 107070.
19. Yang, L., Chen, L., Du, X., Yang, Y. (2013). Effects of ambient winds on the thermo-flow performances of indirect dry cooling system in a power plant. *International Journal of Thermal Sciences, 64,* 178–187.
20. Liao, H., Yang, L., Wu, X., Du, X., Yang, Y. (2016). Impacts of tower spacing on thermo-flow characteristics of natural draft dry cooling system. *International Journal of Thermal Sciences, 102,* 168–184.
21. Gu, H., Wang, H., Gu, Y., Yao, J. (2016). A numerical study on the mechanism and optimization of wind-break structures for indirect air-cooling towers. *Energy Conversion and Management, 108,* 43–49.
22. Khamooshi, M., Anderson, T. N., Nates, R. (2021). A numerical study on interactions between three short natural draft dry cooling towers in an in-line arrangement. *International Journal of Thermal Sciences, 159,* 106505.
23. Jahangiri, A., Borzooee, A., Armoudli, E. (2019). Thermal performance improvement of the three aligned natural draft dry cooling towers by wind breaking walls and flue gas injection under different crosswind conditions. *International Journal of Thermal Sciences, 137,* 288–298.
24. Li, L. (2015). *Thermo-flow performance analysis and optimization of large-scale indirect air-cooling system*. Nanjing, China: Southeast University.
25. Dong, P., Kaiser, A. S., Guan, Z., Li, X., Gurgenci, H. et al. (2019). A novel method to predict the transient start-up time for natural draft dry cooling towers in dispatchable power plants. *International Journal of Heat and Mass Transfer, 145,* 118794.
26. Dong, P., Li, X., Hooman, K., Sun, Y., Li, J. et al. (2019). The crosswind effects on the start-up process of natural draft dry cooling towers in dispatchable power plants. *International Journal of Heat and Mass Transfer, 135,* 950–961.
27. Wu, T., Ge, Z., Yang, L., Du, X. (2019). Transient behavior of the cold end system in an indirect dry cooling thermal power plant under varying operating conditions. *Energy, 181,* 1202–1212.
28. Zhang, L., Li, X., Zhou, J., Yu, Y., Feng, J. (2022). Numerical study of the dynamic response of the natural draft dry cooling tower under crosswind condition. *Case Studies in Thermal Engineering, 34,* 102027.

29. Li, X., Gurgenci, H., Guan, Z., Wang, X., Duniam, S. (2017). Measurements of crosswind influence on a natural draft dry cooling tower for a solar thermal power plant. *Applied Energy, 206,* 1169–1183.
30. Xu, M., He, S., Cheng, J., Gao, M., Lu, Y. et al. (2021). Investigation on heat exchanger arrangement in solar enhanced natural draft dry cooling towers under various crosswind conditions. *Case Studies in Thermal Engineering, 28,* 101505.